

Petrophysical characterization of a heterolithic tidal reservoir interval using a process-based modelling tool

Kjetil Nordahl¹, Philip S. Ringrose² and Renjun Wen³

¹Norwegian University of Science and Technology, Department of Mineral Resources and Engineering, Trondheim N-7491, Norway (Present address: Statoil Research Centre, Rotvoll, Trondheim N-7005, Norway)

²Statoil ASA, Exploration and Production, N-7501 Stjørdal, Norway

³Geomodeling Technology Corp., Suite 230, 633 6th Avenue, SW Calgary, Alberta, T2P 2Y5, Canada

ABSTRACT: Heterolithic lithofacies in the Jurassic Tilje Formation, offshore mid-Norway, consist of three components – sand, silt and mud intercalated at the centimetre scale – and are generally difficult to characterize petrophysically with core and wireline data. A near-wellbore model of the lower part of the Tilje Formation in the Heidrun Field is constructed to illustrate the application of these results to formation evaluation studies. The sedimentological model is developed by detailed parameterization of a cored well interval and the petrophysical properties are based on core plug data, taking into account sampling bias and length scale. The variation in petrophysical properties as a function of sample volume is examined by calculating the representative elementary volume. The sensitivity of the representative permeability values to the contrast between the three components is studied and gives a better understanding of the flow behaviour of this system. These results are used to rescale the core plug data to a representative value and thereby quantify the uncertainty associated with the wireline-based estimates of porosity and horizontal permeability and to give an improved estimate of the k_v/k_h ratio.

KEYWORDS: *petrophysics, permeability, porosity, heterolithic sandstone*

INTRODUCTION

Sedimentary architecture causes heterogeneity at many scales, which can affect reservoir performance (e.g. Haldorsen 1986). At the bedding (sub-metre) scale, primary sedimentary structures can influence the flow properties significantly, as has been shown for a range of sedimentary systems (Weber 1982; Hurst & Rosvoll 1991; Corbett & Jensen 1993; Hartkamp-Bakker & Donselaar 1993). These studies show that porosity and permeability are controlled strongly by depositional processes through their influence on grain size, sorting and fabric. Because of computational limits on the number of grid-cells in reservoir simulation, small-scale sedimentary structures cannot be included explicitly, but have to be represented by effective or representative values.

The problem of integrating data with different sample support in heterogeneous reservoirs has also been appreciated widely (Haldorsen 1986; Enderlin *et al.* 1991; Worthington 1994; Corbett *et al.* 1998). In particular, the integration between core data (usually represented by discrete core plugs) with continuous wireline data is challenging since heterogeneities are often on the same scale as the measurement resolution. To integrate the two datasets, the normal approach is to upscale the measurements with the smallest sample support to the scale of the larger.

Methods for generating numerical models of the subsurface domain are reviewed by Koltermann & Gorelick (1996). Population of these models with petrophysical properties and calculating the effective flow properties at a larger scale can be

done in a variety of ways (Renard & Marsily 1997). For simple geometries (e.g. a stratified medium) exact analytical solutions can be found. In more complex cases, numerical methods can be used to estimate effective properties. Usually, only two component systems (sand and mud) are evaluated (Begg & King 1985; Desbarats 1987; Deutsch 1989; Durlofsky & Chung 1990).

Regardless of the upscaling technique, the question remains as to what scale should the measurements be rescaled. Bear (1972) introduced the concept of Representative Elementary Volume (REV). This is based on effective medium theory, which assumes that the correlation lengths are shorter than the model domain. If the sample support is small compared to the length scale of the heterogeneity, the measured value will vary with a change in the support since varying degree of heterogeneity is included in the sample volume. At some scale (the REV), the fluctuations are minimized and a representative amount of heterogeneity can be measured (Fig. 1).

The tidal deltaic Tilje Formation (Martinius *et al.* 2005), is particularly heterogeneous and exhibits variability at many scales. Brandsæter *et al.* (2001) showed that the ratio between vertical and horizontal permeability (k_v/k_h ratio) was one of the most important parameters influencing oil recovery in this formation. At the bedding scale, thin intercalations of mudstone and sandstone layers have a strong influence on the flow properties (these two lithological components are hereafter referred to as sand and mud). These facies are dominated by heterolithic current ripple bedforms which have been described as flaser, wavy or lenticular bedding (Reineck & Wunderlich

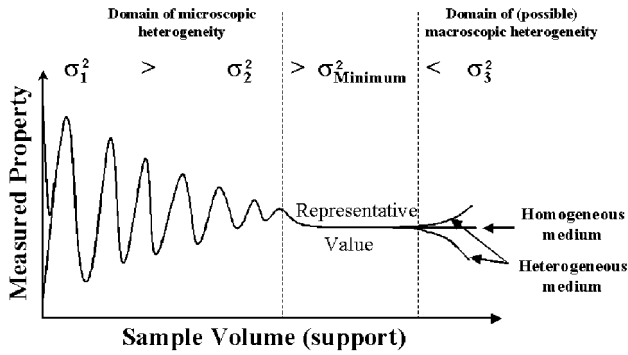


Fig. 1. Concept of Representative Elementary Volume (REV). In this paper, the microscopic domain refers to the scale from lamina to bed set, while the macroscopic domain to a scale larger than the lithofacies (modified after Bear 1972).

1968). Flaser and lenticular bedding represent end-members of a range of tidal bedding types, with discontinuous mud lamina and discontinuous sand ripples, respectively. Wavy bedding

describes more regular interbedding with approximately equal amounts of sand and mud. These millimetre- to centimetre-scale heterogeneities are not well characterized by the core plug or the wireline log measurements. Core plug measurements are at a volume scale below the characteristic length scale of the heterogeneity and the wireline logs tend to average out the responses from the different lithological components present. Integration between these two datasets is, thus, problematic. Figure 2 shows the studied interval of well H1 from the lower part of the Tilje Formation in the Heidrun Field. This figure shows that the petrophysical variability is high, both within and between the different facies associations, such that there is in general a mismatch between the core and the wireline values.

This paper considers these problems using a process-based stochastic modelling tool (SBED™) (Wen et al. 1998). With this method, a realistic near-wellbore model is created. The near-wellbore model is defined here as a numerical representation of the sedimentological components and petrophysical properties in a rectangular shaped volume along the wellbore with a lateral dimension on the scale of the conventional wireline tool resolution. This also corresponds approximately to the lateral

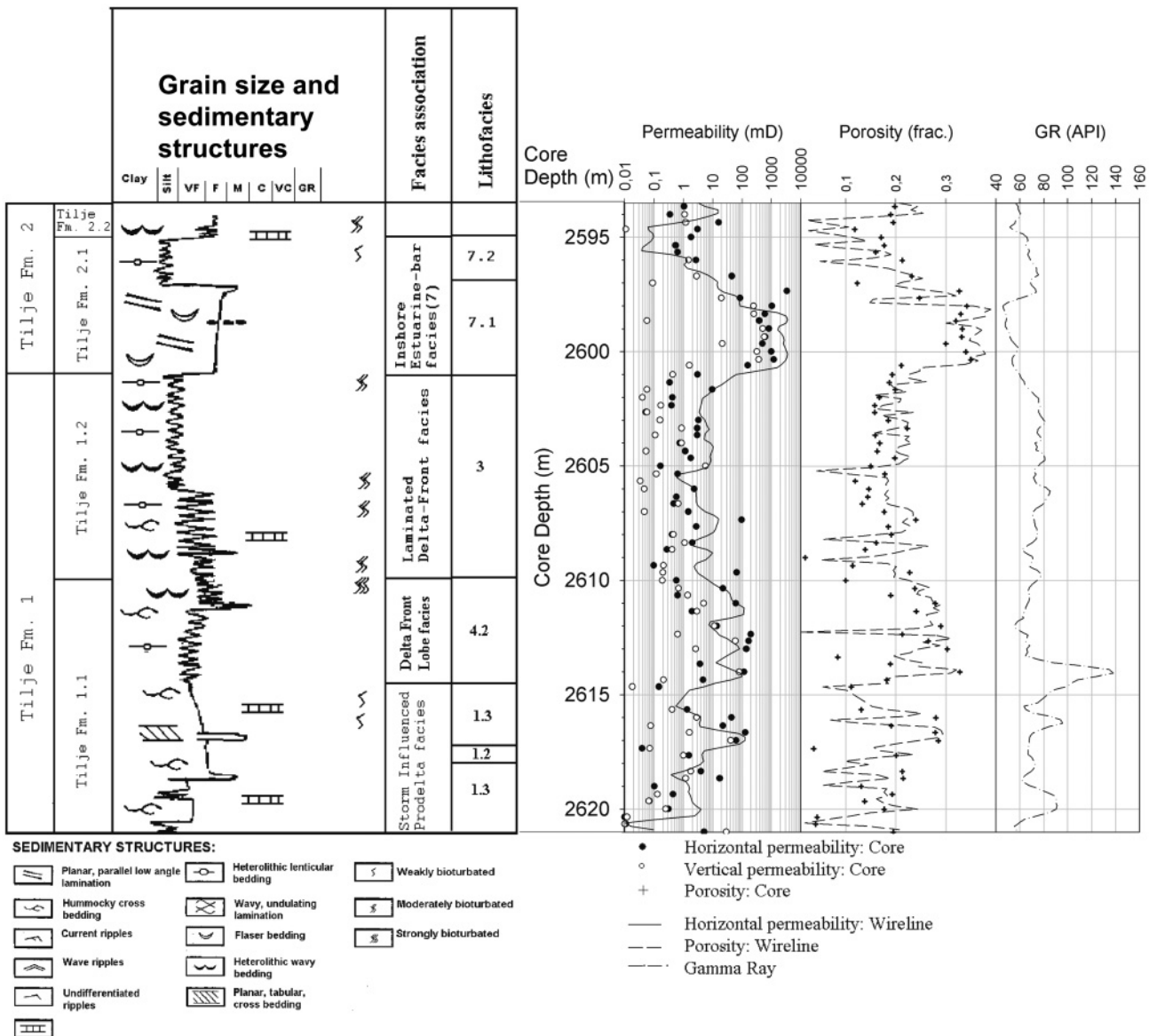


Fig. 2. Core data and wireline estimate from the studied interval in the Tilje Formation. The facies associations are from Martinus et al. (2001).

correlation lengths of the sedimentological and petrophysical elements in tidal facies. To be able to evaluate the tidal bedding system in general, a range of bedding models with different mud contents was created. Permeability is shown to vary with the sample volume and the REV can be calculated on these models. Furthermore, the sensitivity of flow behaviour to the permeability contrast between the different lithological components is explored. Finally, the near wellbore model is used to quantify the uncertainty associated with traditional averaging of core and wireline data to give improved estimates of the petrophysical properties in the studied interval.

THE NEAR-WELLBORE MODEL

Modelling of small-scale (centimetre–decimetre) sedimentological bedforms has been studied widely and pioneering work on synthetic bedform modelling was published by Rubin (1988). The SBED method was developed by Wen *et al.* (1998) and makes a significant step towards a petrophysically useful method by extending the approach of Rubin (1988) to include stochastic elements and 3D property modelling. The method used in SBED is based on manipulation of the following surface function:

$$\tilde{z}(x,y)^t = A \sin\left(\frac{x}{L_x} + \Theta_x\right) + B \sin\left(\frac{y}{L_y} + \Theta_y\right) + g(x,y) \quad (1)$$

where x and y are spatial coordinates, t is a nominal time increment, A and B are amplitudes of the bedform in the current (x) and crest (y) directions, L_x and L_y are wavelengths of the bedform in the current and crest directions, Θ_x and Θ_y are initial phase angles (radians) and $g(x,y)$ is a 2D Gaussian random function. The input parameters to the program describe the bedform morphology in cross-section and plan-view (by a sine-function) and also how the surfaces move in space and time by vectors to mimic bedform migration (Fig. 3a). The displacement creates a 3D volume separated by the surfaces giving a simulated lamina (Fig. 3b). After a sequence of surfaces representing a lamina set, $\tilde{z}(x,y)^{t=n}$, a hiatus is simulated and erosion by a new time series is initiated (i.e. a new lamina set). The migration of bedforms, which in nature is a result of periodic avalanching and suspension fallout on the bedform lee- and stoss-side, is simulated here by displacement of successive sine curves. This is a simpler approach than process-based methods in which grain deposition is simulated. The input parameter set comprises a set of values to give a particular type of sedimentary bedform. The stochastic elements of the code reflect the natural variability in the deposits and ensure that a number of equiprobable realizations of the bedform model can be generated. Figure 3c shows an example of a realization of a geometry model. Statistical parameterization of the sedimentological observations from core gives the opportunity to determine the mean value of the deterministic part of the code while allowing the natural variability to be included in the stochastic elements. Table 1 gives some of the sedimentological parameters considered for this interval. The key parameters are the geometry, thickness variation and frequency of the mud layers, since these will have a strong influence on the vertical and horizontal permeability. Also listed in Table 1 are the main input parameter groups that are used to mimic the depositional process.

Within this geometrical bedding framework, petrophysical properties (porosity and permeability) are simulated using correlated 2D Gaussian random fields. On the resulting permeability grid (Fig. 3d), directional flow is simulated numerically by imposing a constant head gradient between

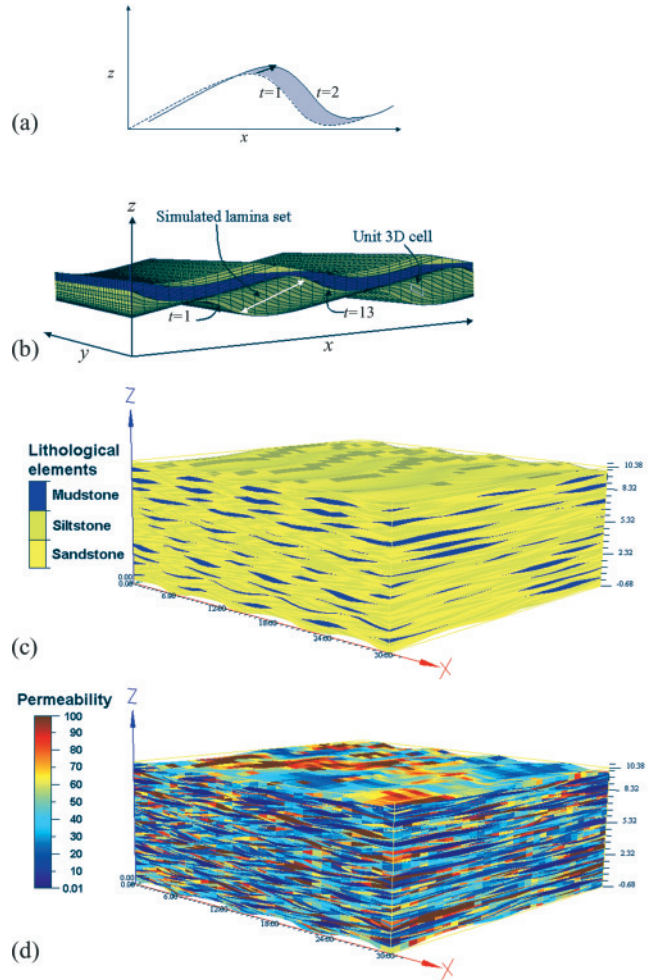


Fig. 3. (a) Schematic sketch of the generation of lamina surfaces in SBED between the $t=1$ and $t=2$ in the time series of equation (1). The grey area is the preserved lamina and the arrow indicates the vector that displaces the surface to mimic bedform migration. Note that the y -direction is not shown and that the preserved lamina is a 3D volume. (b) Simulated 3D sand and mud lamina set in SBED. (c) A realization of a sedimentological model. The three different lithological components present in the geometrical model can be clearly seen; sandstone (yellow), siltstone (brown) and mudstone (blue). (d) A realization of a permeability model. The model size in (c) and (d) is $30 \times 30 \times 10$ cm.

Table 1. Recorded sedimentological core data (left) and main input parameter groups in SBED (right)

Core parameters	Geometrical input parameters
Lamina thickness (mean and standard deviation)	Bedform morphology (plan form and cross-section)
Sand/Mud lamina set thickness (mean and standard deviation)	Migration speed and direction
Periodic components (wavelength and amplitude)	Depositional rate and length for sand and mud
Bedding type (i.e. geometry of mud layers)	

opposite sides of the model and no-flow boundaries on the perpendicular sides. The single-phase steady state flow equation is then solved by a finite-difference method (described by Warren & Price 1961; White & Horne 1987; Renard & Marsily 1997). By rotating the boundary condition set-up and repeating the flow simulation, the diagonal elements of the permeability

Table 2. Core statistics for sand and mud lamina set thickness in the selected lithofacies 7.1

Component	Parameter	Core	Simulation
Sand lamina set	n	11	117
	Arithmetic average	20.14	21.1
	Standard deviation	18.64	1.98
	Median	15.9	21
	Mode	N/A	21
	Minimum	2	20.5
	Maximum	59.2	42.2
	Total (cm)	221.5	2468.4
Mud lamina set	n	11	117
	Arithmetic average	0.68	0.421
	Standard deviation	0.35	0.18
	Median	0.8	0.4
	Mode	0.8	0.5
	Minimum	0.1	0.1
	Maximum	1.2	0.9
	Total (cm)	7.5	49.2
Sand fraction		0.967	0.98
Number of mud layers per metre		4.8	4.65

tensor are found (denoted here as k_{xx} , k_{yy} and k_{zz}). Since porosity is an additive property (Narasimhan 1983), the bulk porosity of the bedding model is found simply by taking the arithmetic average of the individual grid-cell values.

In this study only single-phase flow has been considered. However, where sedimentary structures have a significant effect on single-phase permeability, the multiphase effect on permeability is likely to be even greater. Multiphase flow aspects also need to be considered in reservoir studies and Pickup *et al.* (2000) performed two-phase upscaling on similar synthetic tidal bedding models as used here.

Bedding geometry model

The geometrical model represents the sedimentological features observed in the core, such as the lamina and lamina set characteristics (Table 1). After dividing the core into lithofacies, a detailed log of mud content and lamina set thickness distribution within the cored interval was made and these statistics were then used to develop the bedding models. To illustrate the modelling method, lithofacies 7.1 from the upper part of Figure 2 was selected. Ringrose *et al.* (2005) consider the entire interval in Figure 2 for estimation of vertical permeability. The selected lithofacies is interpreted as an accretionary channel bank deposit (Martinius *et al.* 2001) and is dominated by flaser-bedded deposits separated by thicker mud layers. The number and thickness of the mud and sand lamina sets (Table 2) were considered to have an important control on effective permeability. In order to ensure that the near-wellbore model of this lithofacies is realistic, the same parameters were measured on the numerical model. A realistic model is obtained when the two datasets are similar statistically (Table 2). Figure 4 shows part of this interval with one realization of the near-wellbore model. Table 3 gives the petrophysical parameters for this specific facies, while Table 4 gives the geometrical input parameters.

The petrophysical model

Each grid-cell in the model has a constant lateral dimension (1×1 cm) and a vertical dimension related to the lamina thickness (usually at the millimetre scale, see Fig. 3) and is, by definition, an isotropic and homogeneous petrophysical element. The model dimensions are $0.3 \text{ m} \times 0.3 \text{ m} \times 0.3 \text{ m}$

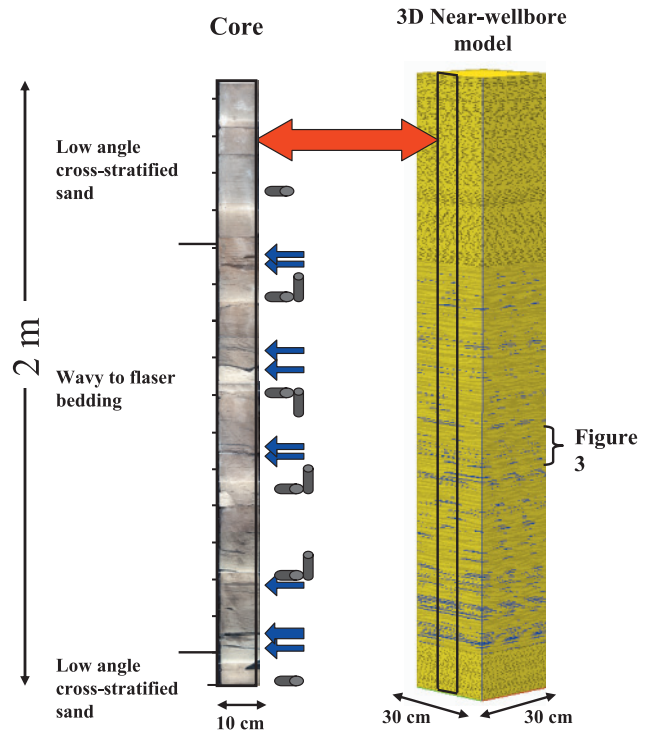


Fig. 4. Core photo and 3D near-wellbore model of the selected lithofacies 7.1 (see Fig. 2 and Table 4). The cylinders indicate the positions of the vertical and horizontal core plugs and the arrows indicate the thick mud layers. Note that the core plugs do not generally sample the mud layers (biased samples).

Table 3. Petrophysical input parameters used; mean (standard deviation)

	Sand component (mD)	Silt component (mD)	Mud component (mD)
Sand-silt contrast 1: 1	100	100	0.01
Sand-silt contrast 1: 2	100	50	0.01
Sand-silt contrast 1: 5	100	20	0.01
Sand-silt contrast 1: 10	100	10	0.01
Sand-silt contrast 1: 100	100	1	0.01
Sand-mud contrast 10^0	100	100	1
Sand-mud contrast 10^{-1}	100	100	0.1
Sand-mud contrast 10^{-2}	100	100	0.01
Sand-mud contrast 10^{-3}	100	100	0.001
Sand-mud contrast 10^{-4}	100	100	0.0001
Sand-mud contrast 10^{-5}	100	100	0.00001
Lithofacies 7.1 (Figs 4, 5 and 11)	Mean ln 6 (0.2) StDev ln 1.2 (0)	Mean ln 4.5 (0.2) StDev ln 1 (0)	0.01 (0)

and consist of $c.$ one million cells. The grid-cell scale is approximately the scale of the probe-permeameter device, $c.$ 2–5 mm (Halvorsen & Hurst 1990; Ringrose *et al.* 2005). One detailed probe-permeability grid was available in the selected lithofacies. The main direct measurements of porosity and permeability are, however, the core plugs. In order to constrain the petrophysical model to data, the process of taking core plugs with 30 cm spacing was simulated from the SBED model. The input petrophysical properties were then adjusted until a match was obtained between the real core plug dataset and the simulated core plug dataset. The simulated core plugs have the same dimension and orientation as the real core plugs and consist of approximately 600–800 grid-cells, depending on the lamina thickness. There are limitations to this approach. First,

Table 4. *Input geometrical parameters for the tidal bedding models; mean (standard deviation)*

Control parameter	MF_0	MF_0.1	MF_0.2	MF_0.25	MF_0.3	MF_0.35	MF_0.4	MF_0.5	MF_0.6	MF_0.7	MF_0.8	MF_0.85	MF_0.9	Example facies (Figs 4 and 11)
Bedform_1 wavelength	20 (1)	20 (1)	20 (1)	20 (1)	20 (1)	20 (1)	20 (1)	20 (1)	20 (1)	19 (0.9)	18 (0.8)	12 (0.7)	9 (0.1)	20 (1)
Bedform_1 amplitude	0.2 (0.05)	0.2 (0.05)	0.2 (0.05)	0.2 (0.05)	0.2 (0.05)	0.2 (0.05)	0.2 (0.05)	0.2 (0.05)	0.2 (0.05)	0.19 (0.045)	0.18 (0.04)	0.12 (0.035)	0.1 (0.01)	0.2 (0.05)
Bedform_2 wavelength	18 (0.5)	18 (0.5)	18 (0.5)	18 (0.5)	18 (0.5)	18 (0.5)	18 (0.5)	18 (0.5)	18 (0.5)	17 (0.45)	15 (0.4)	10 (0.035)	8 (0.03)	18 (0.5)
Bedform_2 amplitude	0.18 (0.05)	0.18 (0.05)	0.18 (0.05)	0.18 (0.05)	0.18 (0.05)	0.18 (0.05)	0.18 (0.05)	0.18 (0.05)	0.18 (0.05)	0.17 (0.045)	0.15 (0.04)	0.1 (0.035)	0.09 (0.001)	0.18 (0.05)
Crest sinuosity_1 wavelength	20 (0.5)	20 (0.5)	20 (0.5)	20 (0.5)	20 (0.5)	20 (0.5)	20 (0.5)	20 (0.5)	20 (0.5)	22.5 (0.5)	25 (0.5)	30 (0.5)	35 (0.5)	20 (0.2)
Crest sinuosity_1 amplitude	5 (0.2)	5 (0.2)	5 (0.2)	5 (0.2)	5 (0.2)	5 (0.2)	5 (0.2)	5 (0.2)	5 (0.2)	4.5 (0.2)	4 (0.2)	3 (0.2)	2 (0.2)	5 (0.5)
Crest sinuosity_2 wavelength	30 (0.6)	30 (0.6)	30 (0.6)	30 (0.6)	30 (0.6)	30 (0.6)	30 (0.6)	30 (0.6)	30 (0.6)	32.5 (0.6)	35 (0.6)	37.5 (0.6)	40 (0.6)	30 (1)
Crest sinuosity_2 amplitude	3 (0.3)	3 (0.1)	3 (0.1)	3 (0.1)	3 (0.1)	3 (0.1)	3 (0.1)	3 (0.1)	3 (0.1)	2.75 (0.1)	2.5 (0.1)	2 (0.1)	1.5 (0.1)	3 (0.05)
Depositional rate: sand	0.3 (0.01)	0.3 (0.01)	0.25 (0.01)	0.235 (0.01)	0.225 (0.01)	0.21 (0.01)	0.2 (0.01)	0.175 (0.01)	0.15 (0.01)	0.125 (0.01)	0.1 (0.01)	0.08 (0.01)	0.07 (0.01)	0.3
Depositional length: sand	4 (0.1)	3.5 (0.1)	3 (0.1)	2.85 (0.1)	2.75 (0.1)	2.6 (0.1)	2.5 (0.1)	2.25 (0.1)	2 (0.1)	1.75 (0.1)	1.5 (0.1)	1.25 (0.075)	1 (0.05)	70 (0.1)
Depositional rate: mud	0 (0)	0.1 (0.01)	0.14 (0.01)	0.155 (0.01)	0.16 (0.01)	0.17 (0.01)	0.18 (0.01)	0.2 (0.01)	0.22 (0.01)	0.24 (0.01)	0.25 (0.01)	0.26 (0.01)	0.27 (0.01)	0.1
Depositional length: mud	0 (0)	3.5 (0.1)	4 (0.1)	4.15 (0.1)	4.25 (0.1)	4.4 (0.1)	4.5 (0.1)	4.75 (0.1)	5 (0.1)	5.25 (0.1)	5.5 (0.1)	5.75 (0.1)	6 (0.1)	7.5 (1)
Average (std dev) sand fraction	1 (0)	0.922 (0.003)	0.804 (0.008)	0.744 (0.008)	0.715 (0.008)	0.658 (0.01)	0.612 (0.01)	0.5 (0.09)	0.391 (0.009)	0.273 (0.011)	0.198 (0.014)	0.125 (0.09)	0.081 (0.09)	0.985 (0.12)

Note: The bedform morphology parameters have dimensions in centimetres, while the depositional parameters are relative length and rate. The variability were modelled with a spherical variogram with range 3 cm for all the parameters. MF, mud fraction.

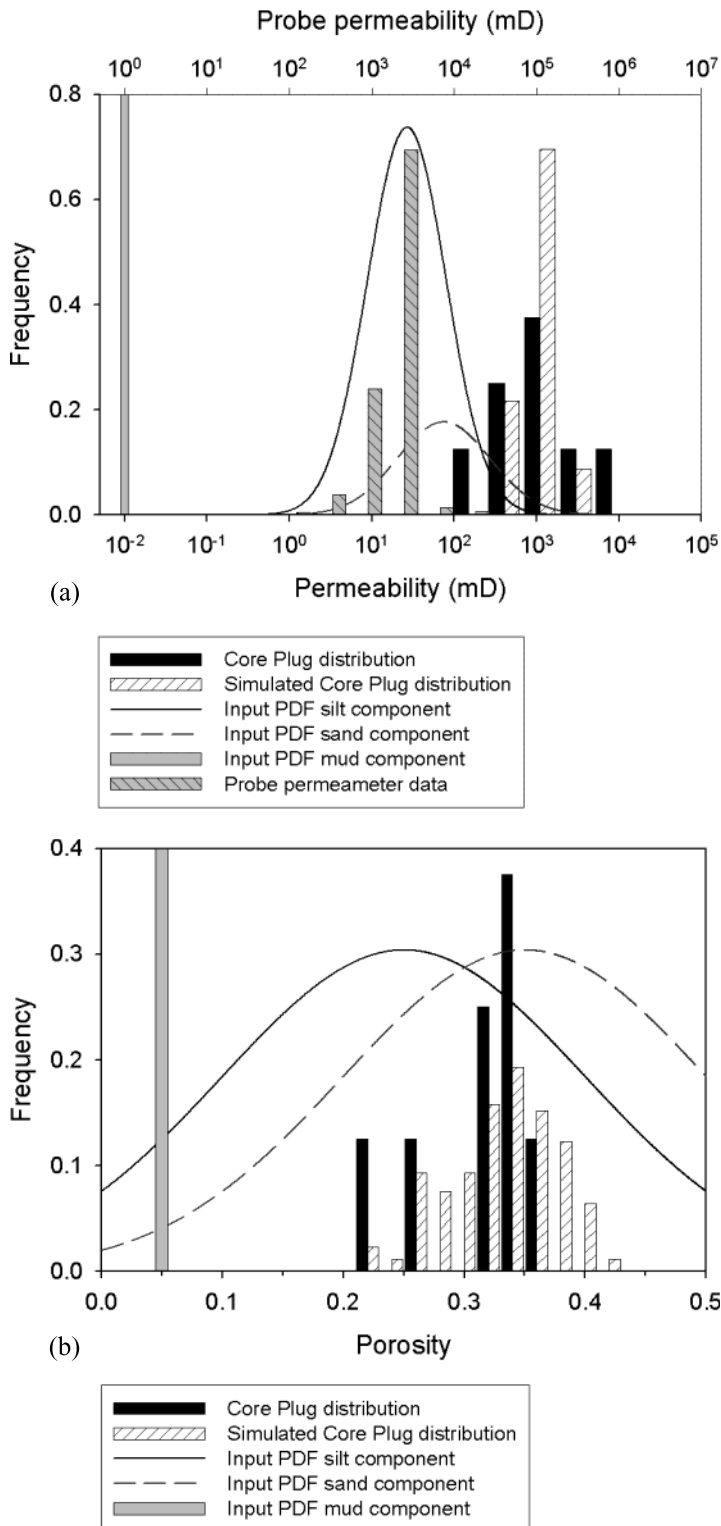


Fig. 5. Comparison between the core plug data (black bars) and the simulated core plugs (cross-hatched bars) for (a) horizontal permeability and (b) porosity. The solid (silt) and dashed (sand) curves show the input distributions that were used to obtain the simulated core plug distribution. The input porosity distribution was truncated at 50% porosity. The mud component was given a low and constant value (grey bar). In addition, inserted in (a) is the probe-permeameter distribution, which has approximately the same variability as the input sand and silt curves.

there should be a sufficient number of real core plugs from each facies to produce a stable histogram. Secondly, the real core plugs are often taken from the more sand-rich zones, avoiding the mud layers (see Fig. 4), but the simulated core plugs are unbiased. Thirdly, several solutions are possible by changing the mean or variance of the input distribution (i.e. the solution is not unique). This is especially the case for porosity. The input permeability has to match both the upscaled vertical and horizontal core plug distributions, giving a better constraint to the options available. Figures 5a and b show the results of

this method for horizontal permeability and porosity, respectively, for the selected facies in the interval. There is a good match between the simulated and the real core plug dataset, both validating the petrophysical model and giving the three-component distribution of porosity and (isotropic) permeability. Figure 5a also shows the available probe permeameter data and the distribution is similar to the distribution of the sand and silt components. Table 3 gives the petrophysical parameters for these curves and Figure 4 shows a realization of the final bedding model for the selected facies.

Even though there is an acceptable match between the core plug values and the model results, the latter tend to have slightly lower variability than the former. This is mainly because it is not possible to include all natural variability in geometry and petrophysics. For example, diagenetic features and fractures are not included in the synthetic bedding models. Although the Tilje Formation in the Heidrun Field is not severely affected by diagenesis, in other cases diagenesis could be equally important as the influence of the primary sedimentary structures. However, it is considered that the near-wellbore model created here captures the most important features affecting the bedding-scale petrophysical properties.

There are few reported measurements on the mud component from these intercalated bedding types, but Ringrose *et al.* (2005) discuss plausible values for mud permeability. A constant value of 0.01 mD is chosen here and then the sensitivity to this parameter on effective vertical and horizontal permeability is evaluated. Although 0.01 mD may be a rather high permeability for mud, for single-phase simulation it is the contrast between the lithological elements that is most important.

PETROPHYSICAL VARIABILITY WITH SAMPLE SUPPORT

Several theories have been developed to estimate effective properties of heterogeneous media. In simple geometrical cases exact solutions exist and, for infinite, continuous parallel layers the horizontal and vertical effective permeabilities are given by the arithmetic and harmonic averages, respectively. In the case of a random, uncorrelated, isotropic lognormal permeability distribution, the geometric average has been shown to give a good estimate (Warren & Price 1961). Although these estimates are useful, they do not generally apply to real sedimentary deposits, which often show more complex geometry and variability. Effective media theories assume that the heterogeneity can be modelled as an inclusion embedded in a homogeneous matrix. If the inclusion has a simple form, analytical expressions for permeability can be calculated (e.g. Dagan 1979). In percolation theory, assuming two components where one is impermeable and the components are distributed randomly in space, the threshold for flow can be evaluated as a function of the conducting component (e.g. Begg & King 1985). Randomly dispersed shales in a sandstone medium were evaluated numerically by Desbarats (1987), who showed that the effective permeability depends on the shale volume fraction, the spatial correlation structure and the dimensionality of the flow system. Deterministic modelling of sedimentary structures has also been performed (e.g. Corbett *et al.* 1992; Pickup *et al.* 1995; Ringrose *et al.* 1999), where the main focus was on fluvial and aeolian deposits. In these previous studies, only two components (sand and shale or two types of sand) were considered. The assumption of a two-component system is a simplification of tidal deposits since the sand lamina set consists of both sand and silt-sized particles organized as cross-stratification in addition to the mud component. In addition, both the sand and the mud components are highly spatially correlated in these tidal deposits.

When the correlation lengths of the different components are smaller than the model domain, a property measured on a sub-domain will depend on the size, position and orientation of this sub-domain. Bear (1972) showed that at some sample support (the REV), the variability is minimized and a representative property could be measured (Fig. 1). Norris & Lewis (1991) calculated in 2D the representative elementary area (REA) for a range of tidal facies based on binary images of an

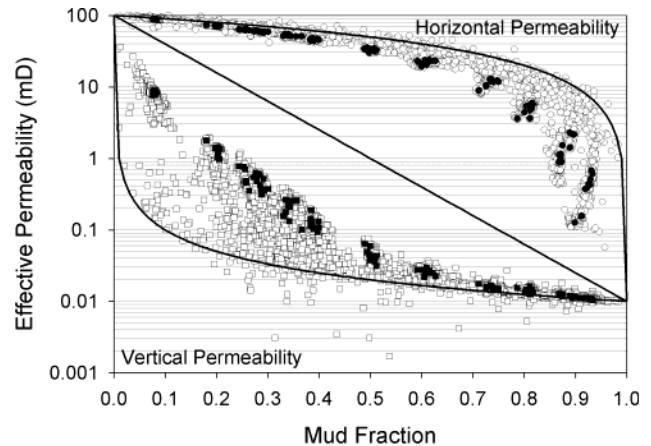


Fig. 6. Simulated horizontal (k_x , white circles) and vertical (k_z , white squares) permeability, representing different sample volumes and mud contents (total of 3600 data points). The values measured at the REV are marked by black squares (k_x) and circles (k_z). The solid lines represent the harmonic, geometric and arithmetic averages.

outcrop sample and found that for horizontal permeability the same REA applied regardless of the mud content. Jackson *et al.* (2003), dividing heterolithic rock cubes into smaller samples, showed that the effective property in 3D could be estimated with simple averaging schemes and that the choice of estimator depended on bedding type.

In order to evaluate the fundamental properties of the heterolithic bedding system, a set of models with different mud fraction was developed, ranging from sand-dominated flaser bedding to mud-dominated lenticular bedding. Baas (1994) studied the development of ripple morphology in unidirectional flow using flume tank experiments and found that ripples approached an equilibrium size and shape with either increasing current velocity or depositional time. Oost & Baas (1994) also evaluated the effect of unsteady flow (common with tidal currents) in the bedform morphology development. These experimental results have been used to constrain the input parameters for the numerical model, thereby obtaining realistic geometries. The geometrical input parameters for these general tidal bedforms are found in Table 4.

First, to evaluate how the petrophysical properties vary with sample support, and to isolate the effect of geometry and mud fraction, a two-component system (sand and mud) was used, where the petrophysical contrast between the components was constant and equal to 10^4 (sand permeability of 100 mD and mud permeability of 0.01 mD). Smaller sub-models were then extracted from the larger-scale model in a systematic manner, where the sub-grid size (i.e. sample volume) is increased in a cubic series (in 30 steps) from the smallest sample in the centre of the realization to the full size (0.3^3 m^3). There was no observed dependency on the location of the centre point of the sub-grids. The effective permeability for each sub-grid was then calculated for the vertical direction (k_z) and in the horizontal direction along the migration direction for the ripples (k_x). A total of 12 different bedding models (with ten realizations of each) with varying mud content were used and Figure 6 shows all the results from the simulation where each square represents a specific mud content and sample volume. Note that there is a larger spread in upscaled permeability (more than two orders of magnitude) for certain ranges, namely below 40% mud fraction for vertical permeability and above 70% mud fraction for horizontal permeability. This indicates that the effective permeability is dependent on the sample size in these mud fraction ranges. Figure 7 shows the effective vertical permeability vs.

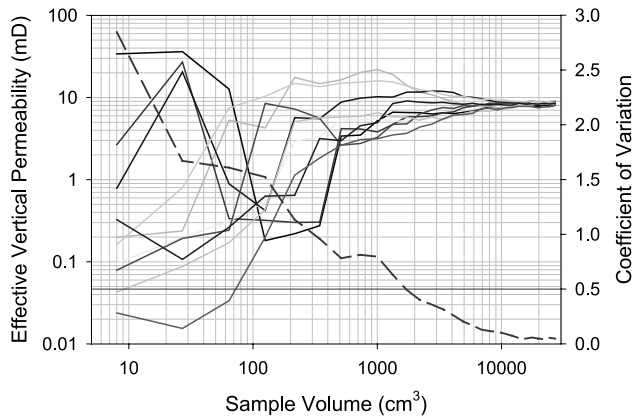


Fig. 7. Example of variation in vertical permeability with sample volume in a low mud content (10%) flaser-bedded model. Each solid line represents one realization and the dashed line is the coefficient of variation (C_v) curve calculated between the ten realizations at each volume step. At volumes larger than about 2000 cm^3 , the C_v value becomes lower than 0.5.

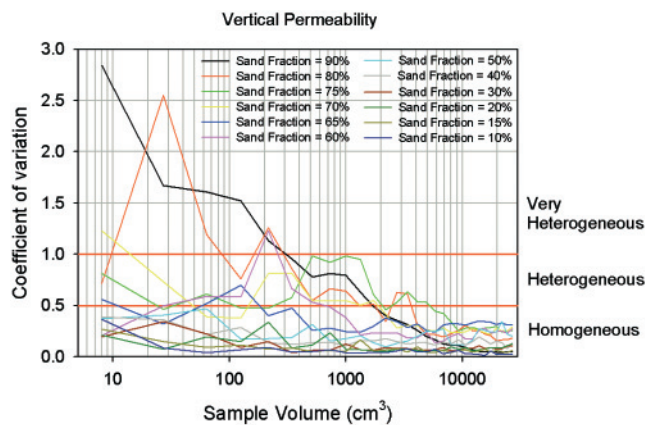


Fig. 8. The C_v curve for vertical permeability for 12 different tidal bedding models with varying mud fraction. Each C_v -line is based on similar calculations as used in Figure 7.

sample volume for one of these models; a flaser-bedded model with 10% mud fraction where the mud occurs as isolated lenses between the sand lamina sets. Each solid line represents one realization. This example clearly shows that the largest variability occurs at small sample volumes and that the fluctuations are minimized at large scales, consistent with the REV concept outlined above. For each sub-grid size, the coefficient of variation (C_v) was calculated between the realizations (see Jensen *et al.* 1997, for fuller discussion of use of C_v for petrophysical analysis). As proposed by Corbett & Jensen (1992), a C_v below 0.5 indicates a statistically homogeneous medium, while above 1 the samples can be considered very heterogeneous. It is observed (Fig. 7) that the C_v decreases as the sample size (sub-grid size) increases, indicating that the effective property approaches the REV. Note that this REV is related only to geometrical heterogeneity and that spatial correlation in permeability will be likely to increase the absolute size of the representative volume. Similar curves as in Figure 7 were obtained for all the other 11 tidal bedding models and the results for vertical permeability are shown in Figure 8, where it can be seen that the sample volume (for $C_v < 0.5$) varies with mud content (this is in contrast to the conclusion of Norris & Lewis 1991). For vertical permeability (Fig. 8) there is a steady increase in this inflection point with increasing mud content,

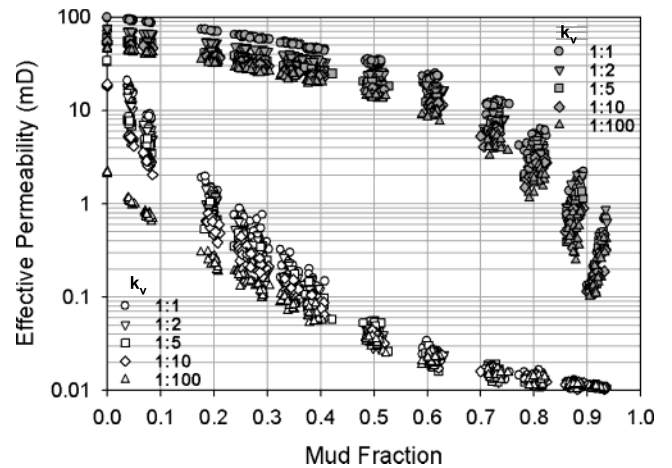


Fig. 9. Effective vertical (white) and horizontal (grey) permeability, with varying contrast between the sand and silt component (constant mud permeability). The plot is based on 240 realizations all at a REV scale. See Table 3 for petrophysical input parameters.

but above 40% mud, all the C_v curves lie in the homogeneous region. This behaviour is related to percolation theory, which predicts the point at which one component will start to connect across the model domain. The change in variability expressed with the C_v curve is related to the change in correlation lengths of sand and mud lenses with respect to the model domain. Further analysis of porosity and horizontal permeability is given in Nordahl (2004) where the issues of stationarity, correlation lengths, percolating thresholds and how to define REV on these bedding models are discussed. The permeability values measured at the REV are indicated in Figure 6 by black squares. It is clear that the representative effective permeability trends deviate significantly from the commonly used arithmetic and harmonic averages, which only are correct in the case of a perfectly stratified medium. The effective permeability of the more realistic and complex models used here can, thus, not be estimated properly with these estimates. Ringrose *et al.* (2003, 2005) discuss different methods that can be used to describe this trend.

EFFECT OF PETROPHYSICAL CONTRAST IN A THREE-COMPONENT SYSTEM

The previous results were for a two-component system (sand and mud) and the variability observed as a function of sample support was a result only of the geometry of the two components. As mentioned above, most of the sand lamina sets in the Tilje Formation consist of (at least) two different grain size classes. Petrophysically, these facies can then be treated as a three-component system. In this section, the effect of changing the petrophysical contrast between the two sand components (contrasting lamina) is evaluated and then, keeping this contrast constant, the effect of different permeabilities of the mud layers is assessed.

Effect of contrast between sand components

The effect of varying the petrophysical contrast within each sand lamina set (Table 3) is evaluated by keeping the permeability of one of the sand components constant and equal to 100 mD and decreasing the permeability of the other component (the silty component). In this case the largest sample volume for each realization was used, such that in all cases the REV was reached ($C_v < 0.5$). In Figure 9, the effective vertical

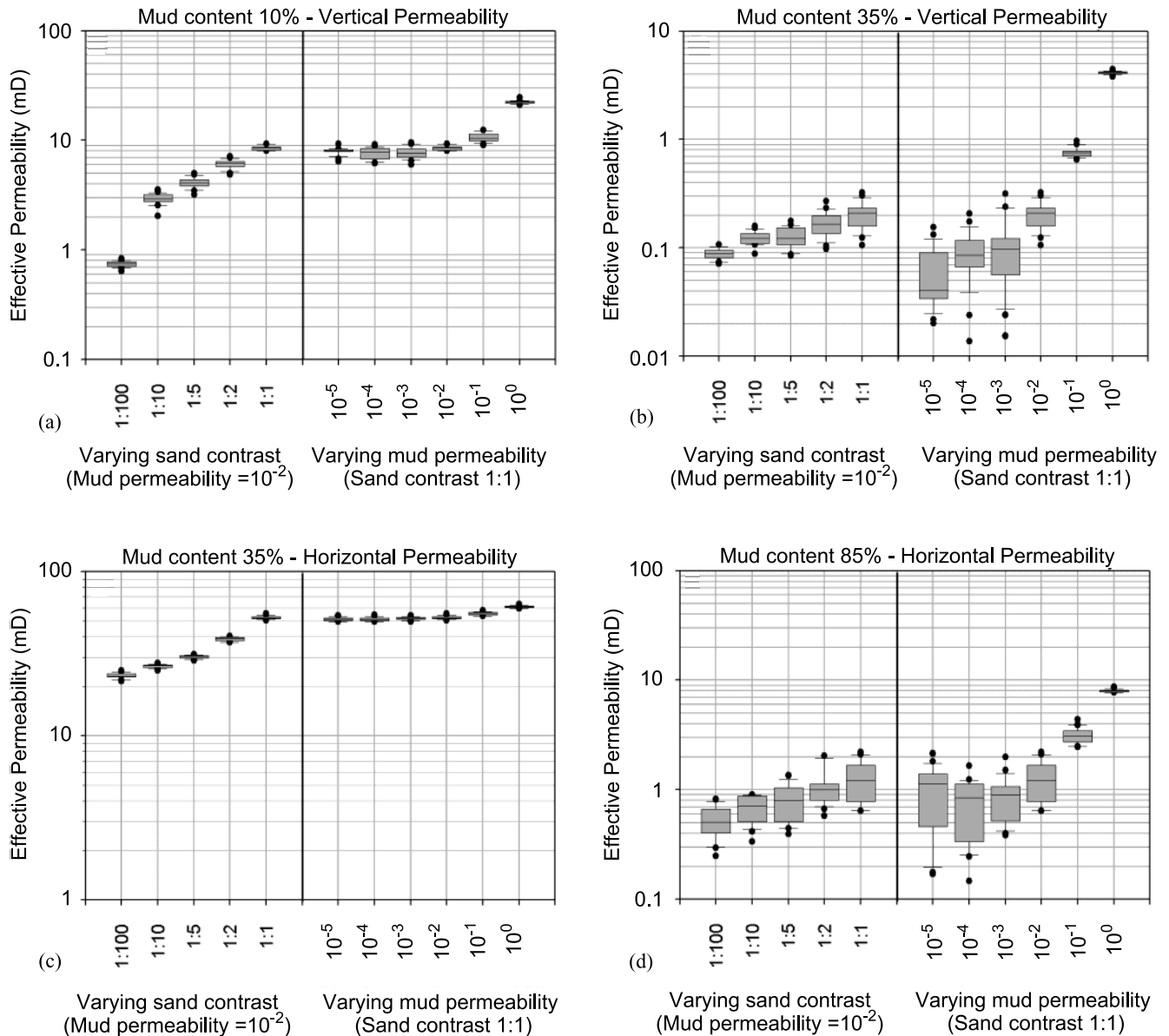


Fig. 10. Effect of changing the mud permeability. Also inserted are the relevant results from Figure 9. Three mud fraction models are used: (a) low mud content case (10%); (b) and (c) near the percolating threshold for vertical flow (35%); and (d) a high mud content (85%) lenticular-bedded model near the percolation threshold for horizontal flow. See Table 3 for petrophysical input parameters.

and horizontal permeabilities are plotted against the mud fraction for the different contrast cases. In the low mud range, effective permeability is closely related to mud fraction and follows clear separate trends for each contrast case. For vertical permeability there is a change at around 40–50% mud content, where the different cases merge towards one curve. The data for horizontal permeability have similar characteristics; however, the convergence of the five contrast cases occurs at around 80% mud fraction. This is again related to the percolation threshold and will be discussed below. Desbarats (1987) found similar threshold values using a markedly different two-component model.

Effect of contrast between sand and mud

The petrophysical properties of the mud layers and, especially, the permeability, are difficult to measure and represent a large uncertainty. To evaluate this uncertainty, the contrast between the sand and silt component was kept constant (and equal to 1)

and the mud permeability varied from 10^{-5} to 10^0 in six steps (Table 3). The models with mud content of 10%, 35% and 85% were used to evaluate the effects in different flow regimes. The results are plotted in Figures 10a–d, along with a summary of the study of varying the contrast within sand lamina set (from Fig. 9). In the case with only 10% mud, the vertical permeability is dominated by the magnitude of the contrast between the sand components and almost unaffected by varying the mud permeability (Fig. 10a), meaning that the mud lenses only act as weak baffles to the vertical flow. The same was found for horizontal permeability (not shown). Near the percolation threshold for vertical flow (35% mud), vertical permeability shows a strong dependency on the mud permeability (Fig. 10b), while horizontal permeability is only affected weakly by the contrast between the sand components (Fig. 10c). However, at higher mud contents (85%, Fig. 10d), the sand ripples start to disconnect in the horizontal plane, meaning that the percolation threshold for horizontal flow is reached. This gives a higher sensitivity to mud properties and less to the variation in

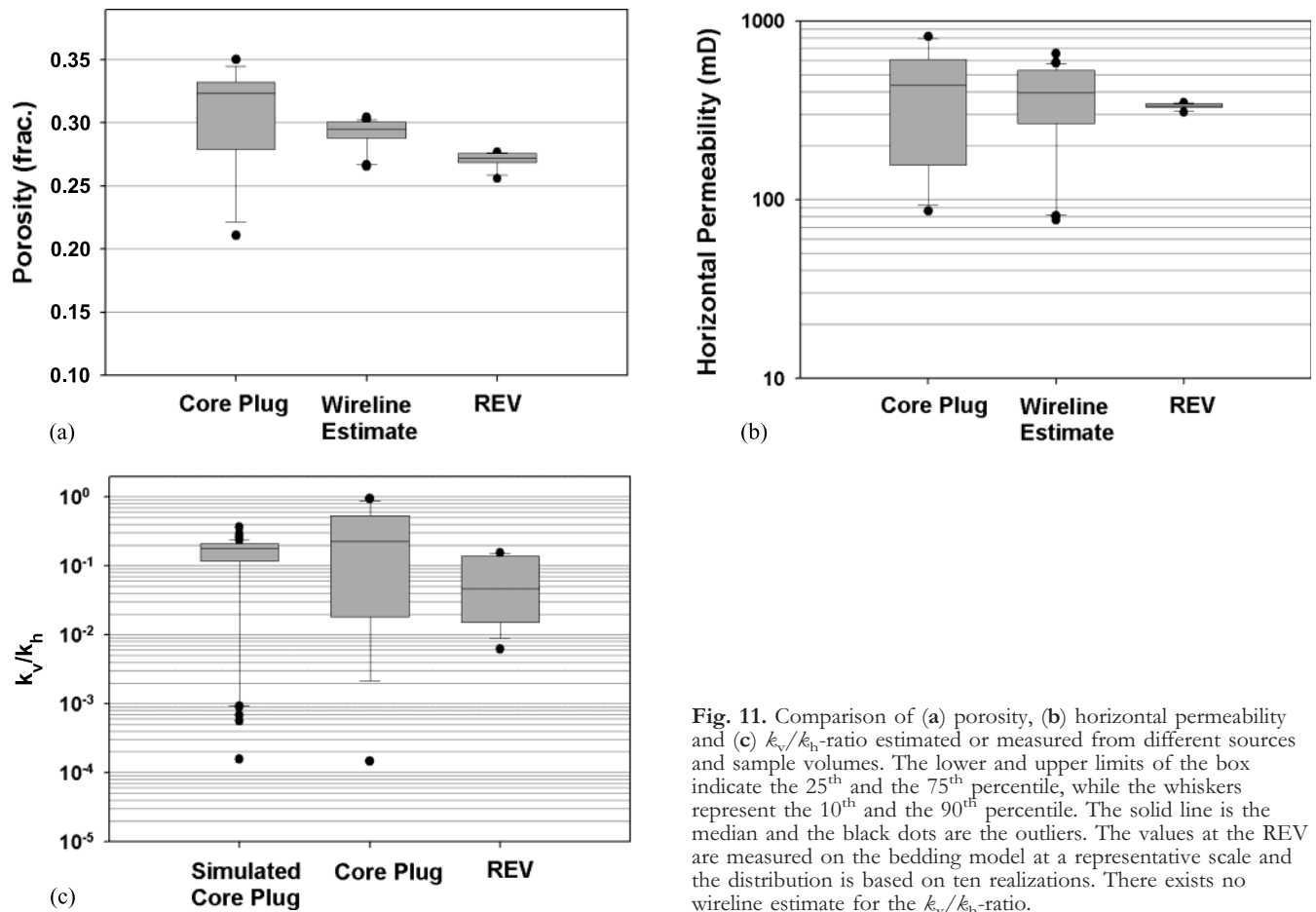


Fig. 11. Comparison of (a) porosity, (b) horizontal permeability and (c) k_v/k_h -ratio estimated or measured from different sources and sample volumes. The lower and upper limits of the box indicate the 25th and the 75th percentile, while the whiskers represent the 10th and the 90th percentile. The solid line is the median and the black dots are the outliers. The values at the REV are measured on the bedding model at a representative scale and the distribution is based on ten realizations. There exists no wireline estimate for the k_v/k_h -ratio.

permeability contrast within sand lamina set. The results above clearly show how effective permeability in complex, heterolithic deposits can be understood with respect to connectivity of sand and mud lamina sets. That is, concepts from both effective medium theory and percolation theory must be used to assess this system properly. These results also indicate that the data collection should be linked with the bedding type. For example, close to and below the percolation thresholds, which are very different for vertical and horizontal flow, mud properties have most influence on effective permeability, while the contrast between the cross-stratified components are more important above the percolating threshold.

ERROR ASSOCIATED WITH WIRELINE ESTIMATES

An important application of these results is that the uncertainty associated with the wireline estimates of porosity and horizontal permeability can be evaluated. Porosity is usually estimated by using a neutron or density wireline log with a calibration to the core porosity. Although porosity is not an extensive property, it is volume-normalized and, consequently, additive (Narasimhan 1983). Since the wireline tool physically measures quantities closely related to the total porosity (e.g. Hook 2003), the integration between core porosity and the wireline tools often is quite reliable. However, in heterolithic deposits, the core plugs tend to be a biased sample (see Fig. 4) since the mud layers are only sampled occasionally and this may influence the integration adversely. A traditional method to estimate horizontal permeability is to establish a regression equation between core porosity and core permeability and use

this to estimate wireline permeability from the wireline estimate of porosity or by the use of some semi-empirical equations. Permeability, being an intensive, non-additive property will, in general, be unpredictable with respect to porosity. This is especially the case when the sample support is very different, as in the case of core plugs and wireline tools, and when the scale of heterogeneity is between these two volume scales. With the SBED tool, porosity and permeability input distributions are taken directly from core plugs, probe permeameter measurements or thin sections and assigned for each lamina and then rescaled to the scale of interest with a realistic bedding model; this method addresses the uncertainty in the wireline estimate.

To illustrate this, models of lithofacies 7.1 have been used. This facies is from the upper part of the studied interval, which is a dominantly flaser-bedded facies with some thicker mud layers separating the different sets (see also Figs 2 and 4 and Table 2). The near-wellbore model of this facies was evaluated at a scale large enough for representative properties to be obtained (in this case 10^6 cm^3). Figure 4 shows the core photo with the positions of the core plugs and the thicker mud layers characteristic of this facies indicated. Note that the core plugs, in general, miss the mud layers, giving a biased dataset.

Although porosity is an easier parameter to estimate, the bias in the core plug dataset towards sand properties will influence the calibration process with the wireline tool. Figure 11a shows the distribution of the core plugs, the wireline estimate and a dataset measured on a representative scale from the near-wellbore model. In accordance with the REV concept, a reduction in the variance is observed when going from the

measures representing the smallest volume to the largest. However, due to under-sampling of the mud layers, the correct and representative porosity value is somewhat lower. In this case, the error is not large compared with the wireline estimate, but it illustrates well the problem with biased sampling.

Figure 11b shows the result for horizontal permeability. In such a low-mud content facies, the dependency of the mud properties on horizontal permeability is small (see also Fig. 10c). However, by using the estimate made at a representative scale, the variance in the dataset is reduced, thereby giving a less uncertain estimate of this property.

The ratio between vertical and horizontal permeability (k_v/k_h) is both a difficult property to measure and an important property in reservoir simulation (Brandsæter *et al.* 2001). This parameter is particularly sensitive to the geometry and the petrophysical properties of the mud layers. There is no wireline estimate for this property and estimates from production data are often uncertain. However, by using the near-wellbore model, a representative value for k_v/k_h for this facies can be found. Figure 11c shows that this estimate is lower than the estimate from core plug data, which is expected because of the bias in this dataset. The minimum value of the simulated k_v/k_h ratio is higher than the minimum value from core plugs. This is because the few mud layers sampled (by the core plugs) are continuous in the sample but are discontinuous at the scale of the model. This difference in mud layer continuity from core plugs to a larger-scale 3D model has also been noted by Jackson *et al.* (2003). The k_v/k_h ratio will be very dependent on the chosen mud permeability, but even with the rather high value used here (0.01 mD), the difference to the core plug estimate is significant.

There are still issues that have to be addressed in the future to reduce uncertainty further. The true properties of the different components – in particular, the mud properties – will be critical and the probe permeameter data can play an important role to assess the sand lamina set variability. To be able to simulate the wireline tool responses directly on the near-wellbore model would greatly advance the basis for an improved integration. Since some of the models of the sedimentological elements have correlation lengths that approach the model size, it would be useful to use more advanced upscaling techniques (e.g. periodic boundary conditions; Durlofsky 1991) to calculate the effective properties. In addition, the effect of multiphase flow in this heterogeneous system is not considered here and should be investigated. As a result, much more work is still required to characterize these heterolithic deposits properly. However, the introduction of the near-wellbore model, common to the sedimentologist, the petrophysicist and the reservoir engineer, is an important step towards a better and fully integrated characterization of these reservoirs.

CONCLUSIONS

Estimation of petrophysical properties in reservoirs where there are large petrophysical variations at the scale of core plugs and wireline logs is challenging. A key element of this paper is that in these heterogeneous reservoir intervals the core plug values cannot be used directly in calibration and integration with wireline data since they represent measurements from a different sample support and a biased sample.

A process-based numerical modelling tool has been used to evaluate the near-wellbore region of a tide-influenced and heterogeneous reservoir interval in the Heidrun Field in the Haltenbanken area, offshore mid-Norway. A method for parameterization of the core data useful for this modelling tool

has been proposed and used successfully to create realistic facies models from the interval. In addition, a method to establish the underlying distributions of a three-component sedimentary system from simulation of core plugs is outlined. The near-wellbore model is used to rescale the core plug data to the scale of interest, giving a better basis for comparing with other well data.

The variation of effective properties as a function of sample support has been evaluated. It is found that the variability is reduced at some sample volume and that the size of this volume was dependent on the mud content. The trends observed between representative permeability values and mud fraction are related to the percolation thresholds. By changing the contrast between the sand components and between the sand and the mud, different sensitivity to these contrasts were identified and this should guide the data collection in the well.

The results were also used to evaluate the uncertainty associated with the wireline estimates. The k_v/k_h ratio is often the most difficult parameter to estimate from available well data and this paper has shown how a better and less uncertain estimate can be made. Ringrose *et al.* (2005) discuss the estimation of vertical permeability both in the Heidrun Field and in the deeper buried and more complex Smørbukk Field.

The first author thanks the Formation Evaluation Project at the Norwegian University of Science and Technology for financial support. Comments from Inge Brandsæter, Arve Næss, Allard Martinus and Sverre Ola Johnsen during the work are appreciated. The comments from two anonymous reviewers are acknowledged gratefully. Simulations were performed using the SBED™ software package (Geomodeling Technology Corp.). Statoil ASA is thanked for permission to publish the data.

REFERENCES

- Baas, J.H. 1994. A flume study on the development and equilibrium morphology of current ripples in very fine sand. *Sedimentology*, **41**, 185–209.
- Bear, J. 1972. *Dynamics of fluids in porous media*. American Elsevier, New York.
- Begg, S. H. & King, P. R. 1985. Modelling the effects of shales on reservoir performance: Calculation of effective vertical permeability. Paper SPE 13529 presented at the 1985 SPE Symposium on Reservoir Simulation, Dallas, TX, 10–13 February.
- Brandsæter, I., Wist, H.T. & Næss, A. *et al.* 2001. Ranking of stochastic realizations of complex tidal reservoirs using streamline simulation criteria. *Petroleum Geoscience*, **7**, S53–S63.
- Corbett, P.W.K. & Jensen, J.L. 1992. Estimating the mean permeability: how many measurements do you need?. *First Break*, **10**, 89–94.
- Corbett, P.W.M. & Jensen, J.L. 1993. Application of probe permeametry to the prediction of two-phase flow performance in laminated sandstones (lower Brent Group, North Sea). *Marine and Petroleum Geology*, **10**, 335–346.
- Corbett, P. W. M., Ringrose, P. S., Jensen, J. L. & Sorbie, K. S. 1992. Laminated elastic reservoirs: the interplay of capillary pressure and sedimentary architecture. Paper SPE 24699 presented at the 67th SPE Annual Technical Conference and Exhibition, Washington D.C., October 4–7.
- Corbett, P.W.M., Jensen, J.L. & Sorbie, K.S. 1998. A review of upscaling and cross-scaling issues in core and log data interpretation and prediction. In: Harvey, P.K. & Lovell, M.A. (eds) *Core-Log Integration*. Geological Society, London, Special Publications, **136**, 9–16.
- Dagan, G. 1979. Models of groundwater flow in statistically homogeneous porous formations. *Water Resources Research*, **15** (1), 47–63.
- Desbarats, A.J. 1987. Numerical estimation of effective permeability in sand-shale formations. *Water Resources Research*, **23** (2), 273–286.
- Deutsch, C. 1989. Calculating effective absolute permeability in sandstone/shale sequences. *SPE Formation Evaluation*, **4** (3), 343–348.
- Durlofsky, L.J. & Chung, E.Y. 1990. Effective Permeability of heterogeneous reservoir regions. In: Guérillot, D. & Guillon, O. (eds) *2nd European Conference on the Mathematics of Oil Recovery*. Editions Technip, Paris, 57–64.
- Durlofsky, L.J. 1991. Numerical calculation of equivalent grid block permeability tensors for heterogeneous porous media. *Water Resources Research*, **27**, 699–708.
- Enderlin, M.B., Hansen, D.K.T. & Hoyt, B.R. 1991. Rock volumes: Considerations for relating well log and core data. In: Lake, L.W., Carroll, H.B. & Wesson, T.C. (eds) *Reservoir Characterization II*. Academic Press, San Diego, 277–288.

- Haldorsen, H.H. 1986. Simulator parameter assignment and the problem of scale in reservoir engineering. In: Lake, L.W. & Carroll, H.B. (eds) *Reservoir Characterization*. Academic Press, Orlando, 293–340.
- Halvorsen, C. & Hurst, A. 1990. Principles, practice and applications of laboratory mini-permeametry. In: Worthington, P.F. (ed.) *Advances in Core Evaluation: Accuracy and Precision in Reserves Estimation, Reviewed proceedings of the First Society of Core Analysts European Core Analysis Symposium*. Gordon and Breach Science Publishers, London, 521–549.
- Hartkamp-Bakker, C.A. & Donselaar, M.E. 1993. Permeability patterns in point bar deposits: Tertiary Loranca Basin, central Spain. In: Flint, S.S. & Bryant, I.D. (eds) *The Geological Modelling of Hydrocarbon Reservoirs and Outcrop Analogues*. Special Publication of the International Association of Sedimentologists, **15**, 157–168.
- Hook, J.R. 2003. An introduction to porosity. *Petrophysics*, **44** (3), 205–212.
- Hurst, A. & Rosvoll, K. 1991. Permeability variations in sandstone and their relationship to sedimentary structures. In: Lake, L.W., Carroll, H.B. & Wesson, T.C. (eds) *Reservoir Characterization II*. Academic Press, San Diego, 166–196.
- Jackson, M.D., Muggenridge, A.H., Yoshida, S. & Johnson, D. 2003. Upscaling permeability measurements within complex heterolithic tidal sandstones. *Mathematical Geology*, **35** (5), 499–519.
- Jensen, J.L., Lake, L.W., Corbett, P.W.M. & Goggin, D.J. 1997. *Statistics for Petroleum Engineers and Geoscientists*. Prentice Hall PTR, New Jersey.
- Koltermann, C.E. & Gorelick, S.M. 1996. Heterogeneity in sedimentary deposits: A review of structure imitating, process-imitating and descriptive approaches. *Water Resources Research*, **32** (9), 2617–2658.
- Martinius, A.W., Kaas, I., Næss, A., Helgensen, G., Kjærefjord, J.M. & Leith, D.A. 2001. Sedimentology of the heterolithic and tide-dominated Tilje Formation (Early Jurassic, Halten Terrace, offshore mid-Norway). In: Martinsen, O.M. & Dreyer, T. (eds) *Sedimentary Environments Offshore Norway – Palaeozoic to Recent*. NPF Special Publication. Elsevier Science B. V., Amsterdam, 103–144.
- Martinius, A.W., Ringrose, P.S., Broström, C., Elfenbein, C., Næss, A. & Ringås, J.E. 2005. Reservoir challenges of heterolithic tidal hydrocarbon fields (Halten Terrace, Mid Norway). *Petroleum Geoscience*, **11**, 3–16.
- Narasimhan, T.N. 1983. A note on volume-averaging. In: Pinder, G.F. (ed.) *Flow through porous media*. A Computational Mechanics Publication. CML Publications, 46–50.
- Nordahl, K. 2004. *A petrophysical evaluation of tidal heterolithic deposits: application of a near wellbore model for reconciliation of scale dependent well data*. PhD thesis. Norwegian University of Science and Technology, Trondheim, Norway.
- Norris, R.J. & Lewis, J.J.M. 1991. The geological modelling of effective permeability in complex heterolithic facies. Paper SPE 22692 presented at the 66th Annual Technical Conference and Exhibition, Dallas, 6–9, October, 359–374.
- Oost, A.P. & Baas, J.H. 1994. The development of small scale bedforms in tidal environments: an empirical model for unsteady flow and its applications. *Sedimentology*, **41**, 883–903.
- Pickup, G.E., Ringrose, P.S., Corbett, P.W.M., Jensen, J.L. & Sorbie, K.A. 1995. Geology, geometry and effective flow. *Petroleum Geoscience*, **1**, 37–42.
- Pickup, G., Ringrose, P.S. & Sharif, A. 2000. Steady-state upscaling: from lamina-scale to full-field model. *SPE Journal*, **5** (2), 208–217.
- Reineck, H-E. & Wunderlich, F. 1968. Classification and origin of flaser, and lenticular bedding. *Sedimentology*, **11**, 99–104.
- Renard, Ph. & de Marsily, G. 1997. Calculating equivalent permeability: a review. *Advances in Water Resources*, 20(5–6), **20**, 253–278.
- Ringrose, P.S., Pickup, G.E., Jensen, J.L. & Forrester, M. 1999. The Ardoss reservoir gridblock analogue: Sedimentology, statistical representivity and flow upscaling. In: Schatzinger, R. & Jordan, J. (eds) *Reservoir Characterization – Recent Advances*. AAPG Memoir, **71**, 265–276.
- Ringrose, P. S., Skjetne, E. & Elfenbein, C. 2003. Permeability estimation functions based on forward modeling of sedimentary heterogeneity. Paper SPE 84275 presented at the SPE Annual Technical Conference and Exhibition, Denver, Colorado, 5–8 October.
- Ringrose, P., Nordahl, K. & Wen, R. 2005. Vertical permeability estimation in tidal deltaic reservoir systems. *Petroleum Geoscience*, **11**, 29–36.
- Rubin, D.M. 1988. *Cross-bedding, bedforms, and palaeocurrents. Concepts in Sedimentology and Paleontology*. Society of Economic Palaeontologists and Mineralogists Special Publication, **1**.
- Warren, J.E. & Price, H.S. 1961. Flow in heterogeneous porous media. *Society of Petroleum Engineers Journal*, **1**, 153–169.
- Weber, K.J. 1982. Influence of common sedimentary structures on fluid flow in reservoir models. *Journal of Petroleum Technology*, **34**, 665–672.
- Wen, R., Martinius, A.W., Næss, A. & Ringrose, P. 1998. Three-dimensional simulation of small-scale heterogeneity in tidal deposits – a process-based stochastic simulation method. In: Buccianti, A., Nardi, G. & Potenza, R. (eds)(eds) *Proceedings of the 4th Annual Conference of the International Association of Mathematical Geology (IAMG)*. De Frede editore, Ischia, 129–134.
- White, C.D. & Horne, R.N. 1987. Computing absolute transmissibility in the presence of fine-scale heterogeneity. SPE Paper 16011, presented at the 9th SPE Symposium on Reservoir Simulation, San Antonio, TX, 1–4 February, 209–220.
- Worthington, P.F. 1994. Effective integration of core and wireline data. *Marine and Petroleum Geology*, **11** (4), 457–466.